# The role of filament-packing dynamics in powering amoeboid cell motility

Long Miao*†, Orion Vanderlinde*, Jun Liu*‡, Richard P. Grant§¶, Alan Wouterse‖, Katsuya Shimabukuro*, Albert Philipse‖, Murray Stewart§, and Thomas M. Roberts*,**

*Department of Biological Science and ‡Institute of Molecular Biophysics, Florida State University, Tallahassee, FL 32306; §Medical Research Council Laboratory of Molecular Biology, Hills Road, Cambridge CB2 2QH, United Kingdom; and ‖Van't Hoff Laboratory for Physical and Colloid Chemistry, Debye Institute, University of Utrecht, 3508 TB, Utrecht, The Netherlands

Edited by Thomas D. Pollard, Yale University, New Haven, CT, and approved February 2, 2008 (received for review September 6, 2007)

**Although several models have been proposed to account for how cytoskeleton polymerization drives protrusion in cell motility, the precise mechanism remains controversial. Here, we show that, in addition to force exerted directly against the membrane by growing filaments, the way elongating filaments pack also contributes to protrusion by generating an expansion of the cytoskeleton gel. Tomography shows that filament packing in the major sperm protein (MSP) -based nematode sperm-motility machinery resembles that observed with rigid rods. Maximum rod-packing density decreases dramatically as the rods lengthen. Therefore, as filaments elongate, the cytoskeleton gel expands to accommodate their packing less densely. This volume expansion combines with polymerization to drive protrusion. Consistent with this hypothesis, an engineered MSP mutant that generates shorter filaments shows higher filament-packing density and slower movement.**

leading edge | major sperm protein | protrusion

The crawling movement of eukaryotic cells depends on directed lamellipod protrusion, a process linked to actin filament assembly that expands the cytoskeleton gel at the cell's leading edge (1–5). Although several models have been proposed to account for how polymerization drives protrusion, the precise mechanism remains controversial (6). The Brownian ratchet model (4, 6, 7), for example, proposes that addition of new subunits to cytoskeleton filaments in contact with the membrane generates a protrusive force that drives the membrane forward. However, in addition to pushing against the membrane, filaments can also push against one another. Here, we use the motile machinery of amoeboid sperm of *Ascaris suum* to illustrate how the packing of elongating filaments can make a complementary contribution to protrusion by expanding the cytoskeleton gel.

*Ascaris* sperm motility is remarkably similar to that of other crawling cells and involves extension of a filament-packed lamellipod that attaches to the substrate and pulls the trailing cell body forward (8), even though the motility of these cells is based on the assembly dynamics of filaments formed from major sperm protein (MSP) rather than actin. In nematode sperm, lamellipodial protrusion is powered by assembly of MSP filament networks along the leading-edge membrane (8) that is closely analogous to how actin assembly powers protrusion in other cells (1–4). MSP motility is based on a small number of proteins, and this simplicity offers advantages in studying the basic principles of amoeboid motility (8–10). Moreover, leading-edge protrusion can be reconstituted in sperm extracts, where vesicles derived from the leading edge of the lamellipod trigger assembly of a cylindrical meshwork of MSP filaments, called fibers, that exhibit the same organization and dynamics as the MSP cytoskeleton in sperm (11). As each fiber elongates, it pushes its vesicle forward [supporting information (SI) Movie S1] in the same way that localized assembly of the cytoskeleton pushes the leading edge ahead in crawling sperm (8, 11). These MSP-containing fibers resemble the actin "comet tails" generated by parasites such as *Listeria* (1–4).

## Results and Discussion

**Electron Tomography Indicates That MSP Filaments Pack Like Rigid Rods.** Protrusive force in the *Ascaris* sperm *in vitro* motility system is generated by polymerization of MSP filaments that occurs in a narrow zone in the fiber immediately adjacent to the vesicle (12). Electron tomography of semithick sections in this fiber expansion zone showed that the filaments were relatively straight and arranged as a meshwork (Fig. 1*a* and Movie S2) like the actin filaments in tomograms of the leading edge of *Dictyostelium* cells (13). Many MSP filaments had one end abutting the vesicle membrane but then crisscrossed as they extended rearward. Stereological analysis (14) showed no evidence for any preferred filament orientation relative to the fiber axis *SI Text*.

The average length of filaments in tomograms increased with distance from the vesicle and plateaued ≈0.5 $\mu$m from the vesicle surface, indicating that filament elongation is restricted to the region adjacent to the vesicle. By contrast, filament-packing density was highest at the vesicle membrane and decreased with distance from the vesicle surface (Fig. 1 *b* and *c*).

The organization of MSP filaments in fibers resembles that produced by random packing of rigid rods on both macro- and microscales (15–18). The MSP filament persistence length, measured from electron micrographs of negatively stained filaments assembled from purified protein, was ≈9 $\mu$m (*SI Text*). The maximum filament length observed in fibers was only 1.5 $\mu$m, and the average length was 0.67 $\mu$m. Thus, to a first approximation, the filaments can be considered rigid or at least relatively inflexible. The decrease in packing density in fibers associated with MSP filament elongation is consistent with the packing behavior of rigid (15–17) or semiflexible (18) rods, in which the maximum packing density decreases with increasing aspect ratio (length/diameter), so that longer rods pack less densely than shorter ones (15–17).

The effect of rod-aspect ratio on packing density can be illustrated with familiar objects, such as copper wire (Fig. 2*a*),

Author contributions: A.P., M.S., and T.M.R. designed research; L.M., O.V., J.L., R.P.G., A.W., K.S., and T.M.R. performed research; L.M., O.V., J.L., R.P.G., A.W., K.S., A.P., M.S., and T.M.R. analyzed data; and A.W., A.P., M.S., and T.M.R. wrote the paper.

The authors declare no conflict of interest.

This article is a PNAS Direct Submission.

Data deposition: The atomic coordinates have been deposited in the Protein Data Bank, www.pdb.org (PDB ID 2BVU).

†Present address: National Laboratory of Biomacromolecules, Institute of Biophysics, Chinese Academy of Sciences, Beijing 100101, China.

¶Present address: School of Molecular and Microbial Biosciences, University of Sydney, Sydney NSW 2006, Australia.

**To whom correspondence should be addressed. E-mail: roberts@bio.fsu.edu.

This article contains supporting information online at www.pnas.org/content/full/0708416105/DCSupplemental.

© 2008 by The National Academy of Sciences of the USA

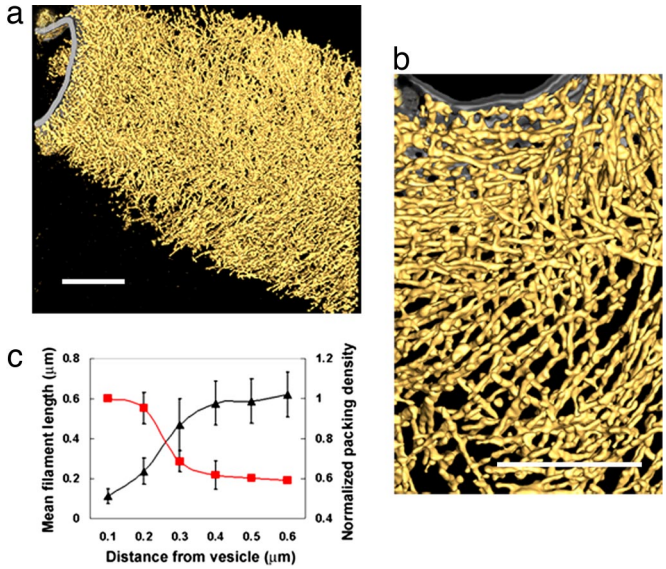


**Fig. 1.** Packing density of MSP filaments in fibers assembled *in vitro*. (*a*) Low-magnification EM tomogram of the growing end of a fiber. Part of the vesicle membrane is shown in gray. The packing density of the filaments (gold) is highest just behind the vesicle. (Scale bar, 0.5 $\mu$m.) (*b*) Higher-magnification view of the vesicle–fiber interface showing the filament arrangement and decrease in packing density distal to the region adjacent to the vesicle. (Scale bar, 0.2 $\mu$m.) (*c*) Mean length (black) and normalized packing density (red) of filaments in fibers as a function of the distance from the vesicle.

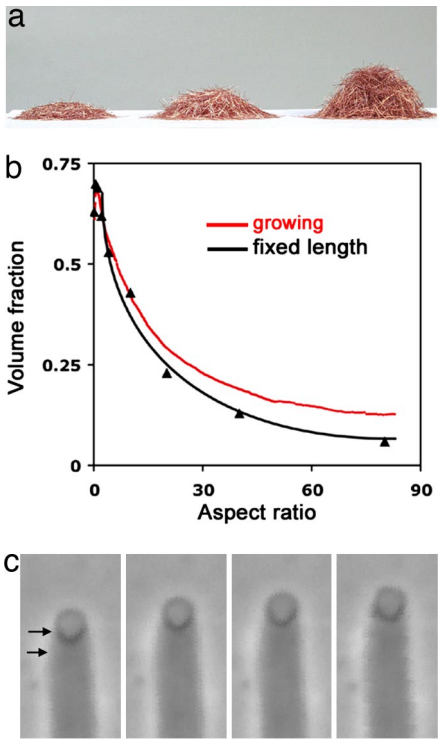


**Fig. 2.** Packing of rigid rods. (*a*) Illustration of how rod length influences packing density. Each pile of rods was formed from 15 g of chopped copper wire, prepared by sprinkling onto a flat surface. The rod lengths were 8, 12, and 16 mm, left to right. The rods in the piles do not stick to one another but, especially the high-aspect ratios, form relatively stiff solid-like entangled structures. The piles were all incompressible. Although the persistence length to contour length ratio of the wire shown here is greater than that of MSP filaments in fibers, similar effects are seen with semiflexible rods (18). (*b*) Simulations indicate that growing rods (red) pack similarly to rods of fixed length (black) and, for both, the volume fraction is approximately inversely proportional to the rod aspect ratio. (*c*) Phase-contrast images taken 5.5 sec apart of the vesicle-bearing end of a fiber growing at an average rate of 8 $\mu$m/min$^{-1}$. The lines indicate the region close to the vesicle where the diameter of the fiber expands, which also moves forward as the fiber grows. (Scale bar, 2 $\mu$m.)

and is due to excluded volume effects, because two objects cannot occupy the same space (19–21). As they lengthen, it becomes progressively more difficult to arrange rods so they do not collide with one another. Consequently, the structure of gels formed from rigid rods differs from that seen with flexible polymers in which the gel properties are dominated by the entropy of the polymer chains (19–21). Although the random way in which growing rods pack is thermodynamically less stable than the liquid-crystal phase, the system is kinetically trapped and so unable to revert to the denser liquid crystal packing (see *SI Text*). Previous studies of rigid-rod packing, using either direct experiment or computer simulations, used only rods of preformed length to establish the relationship of packing density to aspect ratio (15–17). In motile cells, the filaments elongate, which might alter the influence of length on packing density. We investigated this possibility using an extension of the simulation methods developed for fixed length rods (16). These simulations showed that the packing of gradually elongating rods, like that of fixed rods, also achieves a reproducible final maximum packing density that decreases as the rod length increases (Fig. 2*b*).

**Gel Expansion Generated by Packing of Elongating Filaments.** The relationship between filament length and packing density suggests a previously undescribed mechanism by which filament growth contributes to protrusion. MSP polymerizes near the vesicle surface (12). As the filaments elongate, their rotational freedom becomes constrained (19, 20), and they form a coherent gel. As growing filaments move away from the vesicle, they begin to collide with other filaments. Initially, these collisions can be accommodated by local bending, enabling the filaments to pass over one another. However, filament bending stores mechanical energy that can be released by expanding the gel to reduce the packing density. Thus, as filament length increases, the gel volume needs to expand to accommodate the resulting decrease in the maximum density at which filaments can pack. This expansion is reflected by the change in diameter of fibers at their growing end, which increases by an average of 30% ($\pm$12%, $n$ = 34) over the first 1–2 $\mu$m along the fiber axis from the vesicle surface (Fig. 2*c*). Movie S3 shows a molecular dynamics simulation that captures the key features of the organization and dynamics of fibers and illustrates how this gel expansion can generate protrusion (see *SI Text*, Figs. S1–S3). We propose that expansion of the isotropic fiber gel contributes to pushing the vesicle forward, complementing forces produced by polymerizing filaments at the membrane (4, 6).

**Shorter Filaments Pack More Densely and Produce Slower Movement.** To test this hypothesis, we engineered an MSP mutant that produced shorter filaments. We introduced the D83R mutation in a surface loop predicted to be involved in filament assembly (22, 23). This mutant retained the MSP fold (*SI Text*, Table S1). Coassembly of native MSP with bacterially expressed D83R-MSP in 30% ethanol, which induces rapid self-assembly of MSP in the absence of other sperm proteins (24), produced filaments significantly shorter (0.26 $\pm$ 0.15 $\mu$m, $n$ = 392) than those copolymerized from native and bacterially expressed wild-type MSP (0.74 $\pm$ 0.39 $\mu$m, $n$ = 186) (see Fig. S4).

D83R-MSP had a dramatic effect on fiber assembly. Perfusion of growing fibers with cell-free extract (S100) containing D83R-MSP caused an immediate decrease in vesicle velocity, an

CELL BIOLOGY

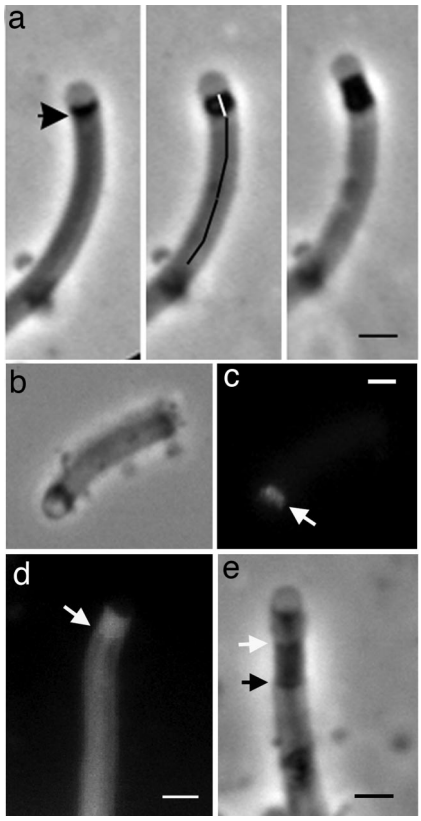


**Fig. 3.** Effect of D83R-MSP on filament polymerization and fiber assembly. (*a*) Sequence of phase-contrast images taken 5 min apart of a fiber grown initially in S100 and then perfused at the point indicated by the arrow with S100 supplemented with 12 mg/ml$^{-1}$ D83R-MSP. The line in the middle indicates the amount of fiber growth 5 min before (black) and after (white) addition of the mutant protein. The presence of D83R-MSP dramatically slowed the growth rate of this fiber (from 0.8 to 0.2 $\mu$m/min$^{-1}$) and resulted in a substantial increase in OD. However, the mutant MSP did not alter the OD of the segment of the fiber assembled before its addition. (Scale bar, 3 $\mu$m.) (*b* and *c*) Paired phase-contrast and fluorescence micrographs of a growing fiber perfused with S100 containing Alexa Fluor 488-labeled D83R-MSP. The labeled mutant protein incorporates into the fiber segment grown in its presence (arrows). (*d*) Fluorescence micrograph of a hybrid fiber grown in the presence of Alexa Fluor 488-labeled native MSP (5 $\mu$M). At the point indicated by the arrow, the fiber was perfused with S100 containing 12 mg/ml$^{-1}$ D83R-MSP together with labeled native MSP. (*e*) Phase-contrast image of a fiber grown in S100 then perfused with S100 containing D83R-MSP (black arrow). Ten minutes later, the fiber was perfused again (white arrow) with S100 without the mutant protein. (Scale bars, 2 $\mu$m.)

increase in OD, and a reduction in diameter at the growing end of the fiber (Fig. 3*a*, Table 1). After addition of D83R-MSP, the entire segment grown in the presence of the mutant protein was dark, and the border between this region and the segment grown before addition remained stationary as the vesicle moved slowly away (Movie S4). When fibers were perfused with S100 containing fluorescently labeled D83R-MSP, the labeled region coincided with the dark, slowly growing segment grown in the presence of mutant protein (Fig. 3 *b* and c), confirming that D83R-MSP incorporated into filaments. Growing hybrid fibers in the presence of fluorescently labeled native MSP confirmed that the increased fiber OD after D83R-MSP addition was due to increased filament mass. Fluorescence intensity in the segment grown in the presence of D83R-MSP was double that in the native segment of the fiber (Fig. 3*d*). The effects of D83R-MSP were fully reversible. When hybrid fibers growing in the presence of the mutant protein were perfused again with S100 lacking

**Table 1. Effect of D83R-MSP on fiber assembly properties**

| | Fiber segment | | Ratio |
|---|---|---|---|
| Property | Native | D83R-MSP† | Native:mutant |
| Growth rate, $\mu$m/min$^{-1}$ | 4.8 ± 1.3‡ | 1.4 ± 0.4 | 3.4 |
| OD (gray value) | 3.3 ± 0.5 | 7.2 ± 0.6 | 0.4 |
| Diameter, $\mu$m | 3.8 ± 1.2 | 3.1 ± 1 | 0.8 |
| Relative polymerzation rate* | 180 ± 48 | 75 ± 18 | 2.4 |

*Relative polymerization rate = ($\Delta V/\Delta t$) × OD; $\Delta V/\Delta t$ = rate of addition of fiber volume with time for a cylindrical fiber with mean diameters and increasing in length at the rates measured for native and D83R segments, respectively.
†[D83R] = 12 mg/ml$^{-1}$.
‡Entries are the mean ± SE for three trials each comprised of ≥ 12 fibers.

D83R-MSP the growth rate, OD, and diameter of the fibers recovered (Fig. 3*e*).

Tomography of hybrid fibers (Fig. 4*a*) showed that, consistent with the effect of the mutant protein on filament length when coassembled with purified proteins, the average filament length in fiber segments grown in the presence of D83R-MSP was less than in adjacent native segments (Fig. 4*b*). Although the exact mechanism by which D83R-MSP modulates filament length is not known, two lines of evidence indicate that D83R-MSP does not simply decrease the rate of filament elongation. First, within segments of fibers grown in the presence of D83R-MSP, the average length of recently assembled filaments located near the vesicle was the same as that of older filaments 3–4 $\mu$m behind the vesicle. Thus, the length of these filaments did not increase with residence time in the fiber. Second, although in principle D83R-MSP could have reduced the number of filaments by inhibiting nucleation, the decrease in filament length in fibers on adding D83R-MSP observed in tomograms (0.24/0.62 $\mu$m = 39%, Fig. 4*b*) was comparable to the decrease in MSP polymerized (42%, Table 1), suggesting that the mutant protein causes premature termination of filament growth, analogous to the way dideoxy nucleotides function in sequencing DNA.

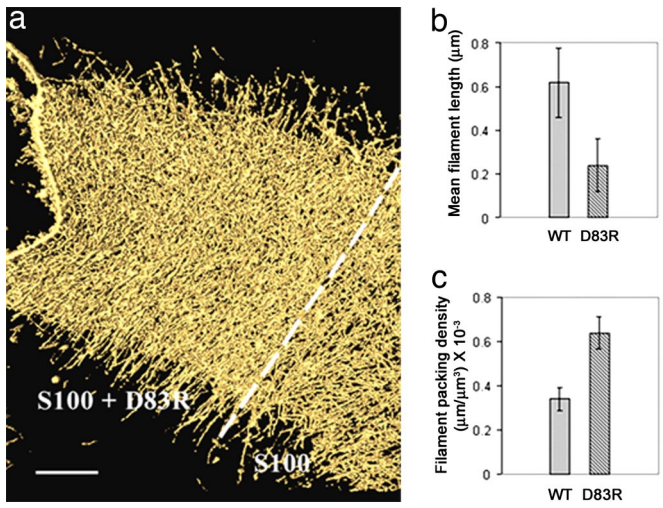


**Fig. 4.** Effect of the D83R MSP mutant on filament length and packing density within fibers. (*a*) EM tomogram of a semithick section of a fiber grown as described in Fig. 3*a*. The dashed line indicates the boundary between segments grown before and after perfusion with S100 containing the mutant protein. (Scale bar, 0.5 $\mu$m.) Measurements from EM tomography showed that perfusion of D83R-MSP into the cell-free motility system resulted in a decrease in average filament length (*b*) and a corresponding increase in filament packing density (*c*). Data points in *b* and *c* represent means (± standard error) from mutant and native segments of five fibers.

Importantly, and in keeping with the doubling of OD and fluorescence intensity observed in this region, the average filament-packing density in the segment grown in the presence of D83R-MSP was almost 2-fold greater than that in the segment grown before mutant protein addition (Fig. 4*c*). Stereology showed that filaments in segments grown in the presence of D83R-MSP, like filaments in native fibers, showed no preferred orientation relative to the fiber axis (*SI Text*). Therefore, the increased OD in fiber segments generated in the presence of D83R-MSP was due to formation of shorter filaments that pack more tightly and not to a change in their orientation within the fiber.

The effects of D83R-MSP on fiber assembly are consistent with the contribution of filament packing to protrusion. Producing shorter filaments resulted in increased packing density, thereby decreasing volume expansion and slowing vesicle movement. Quantitation of the effects of D83R-MSP on fiber growth provided an estimate of the relative contributions of polymerization and filament packing dynamics to vesicle movement (Table 1). Grayscale values obtained by phase-contrast microscopy are proportional to the MSP filament mass in a fiber (see ref. 12 and *SI Text*) and so can be used to determine relative polymerization rates before and after addition of D83R-MSP. Addition of D83R-MSP reduced the relative polymerization rate 2.4-fold (42%). If vesicle movement were due entirely to polymerization, the velocity would decrease accordingly, and packing density (and thus OD) within fibers would not change upon addition of mutant protein. However, D83R-MSP slowed vesicle movement 3.5-fold (Fig. 3*a*). Thus, gel expansion because of packing density dynamics accounts for approximately one-third of the rate of vesicle movement and so considerably augments the effect of polymerization in this system. Such a contribution is also consistent with the ≈30% radial swelling of the native fiber as it moves away from the vesicle. This swelling was not seen with D83R-MSP (Fig. 3*a*). Because D83R-MSP did not alter filament orientation within fibers, this difference cannot be explained by nonproductive polymerization such as formation of filaments too sharply angled to the membrane to push the vesicle. In principle, the changes resulting from addition of D83R-MSP could be explained either by its increasing the attachment of the filaments to the vesicle or by enabling filaments to slide more easily over one another. However, these mechanisms would increase filament- packing density, whereas the packing density observed in D83R tomograms was comparable with that seen in native fibers when the filament lengths were similar (the packing density in native fibers 0.2 $\mu$m from the vesicle, where the filament length was 0.24 ± 0.06 $\mu$m, was 630 ± 60 $\mu m/\mu m^3$ compared with 640 ± 70 $\mu m/\mu m^3$ in mutant fibers). Similarly, if D83R-MSP reduced the elastic modulus of the gel, it could slow motion because of elastic squeezing (25). However, because packing density and filament orientation in mutant fibers was similar to that seen in native fibers, a large change in elastic modulus would seem unlikely. Moreover, such a model would not account for the decreased radial swelling of fibers after addition of D83R-MSP.

**Constraints on the Packing Density Model.** In both MSP fibers and actin-based systems, the polymerization associated with protrusion occurs in a narrow zone within ≈1 $\mu$m of the membrane (1). Cross-linking of filaments in this region could impede changes in packing density associated with filament elongation. Although MSP filaments do form distinctive meshworks in crawling sperm (26) and in cell extracts, and individual MSP filaments do interact sufficiently to bundle spontaneously when assembled from purified protein (27), no MSP cross-linking proteins have been identified. However, several proteins, including $\alpha$-actinin and filamin, cross-link actin filaments, and their properties can be used to consider the influence of cross-linking on filament-packing density dynamics. For example, a 1-$\mu$m-deep filament network at the leading edge would form in ≈6 sec for locomotion rates of ≈10 $\mu$m/min. By contrast, cross-links in actin networks form relatively slowly, on a time scale of minutes (28, 29), considerably slower than the rate at which filaments grow. Moreover, cross-linking proteins appear to be less abundant in the lamellipod compared with bulk cytoplasm (30) and have only micromolar affinity (corresponding to off-rates of 0.1–10 per sec) for F-actin. Thus, few cross-links would be expected to form between rapidly growing actin filaments, and those that did would be transitory on timescales of seconds, thereby allowing filaments in the network to rearrange as they elongated (28, 29). However, once full-length filaments moved away from the leading edge, cross-linking would help stabilize the cytoskeleton so that expansion forces could be used to push more efficiently.

Although there are many similarities between MSP- and actin-based motility, there is an important difference that may influence the extent to which filament packing-mediated gel expansion contributes to actin-driven protrusion. MSP filaments are unbranched (Fig. 1 *b* and *c*). By contrast, in the lamellipods (1–4, 30, 31) of actin-based cells and in actin comet tails (32), the nucleation activity of Arp 2/3 generates a dendritic filament network. These networks of branched entangled filaments differ from the actin gels formed by cross-linking proteins and are likely to have a complex influence on filament packing. Although the mechanical properties of such networks remain to be investigated in detail, intuitively, branch formation should make it more difficult for filaments to pack tightly, accentuating swelling because of excluded-volume packing effects. However, interconnection at branchpoints might also impede the freedom of filaments in the network to move, making it more difficult for them to rearrange to expand the gel, thereby compensating for the increased packing-related expansion of filaments linked by Arp2/3. The extent to which changes in filament-packing density contribute to actin network expansion would also depend on factors such as the rate of debranching (33) and the fraction of the filament mass in the gel formed by Arp2/3-independent mechanisms (such as increasing the number of free barbed ends available for polymerization; ref. 34) that produced filaments that were free to rearrange as they elongated.

**Implications for Cell Motility.** Key properties shared by MSP- and actin-based systems suggest that, although their molecular components differ, the mechanical basis for protrusion may be similar (1, 4, 6, 8–10). Actin filaments have persistence lengths similar to those observed for MSP (35, 36), and the volume fraction occupied by actin filaments in tomograms of motile cells is approximately 6% (13), comparable with that occupied by MSP in fibers. Several models, including thermal (Brownian) tethered ratchets (7), end-tracking mobile clamps (37), nanopropulsion (38), and elastic squeezing (25), have been formulated to explain how actin polymerization drives protrusion. Each has its limitations, and none explains all of the data accumulated from different motility systems (6). The contribution made by filament-packing dynamics we have described in the MSP motility apparatus would complement other mechanisms for generating protrusion and would augment their contribution to motility. Many of these models require that elongating filaments push directly against the membrane, so that only filaments in contact with the membrane contribute to protrusion. In contrast, the contribution made by growing filaments pushing against one another and generating a gel expansion by reducing packing density does not require all growing filament ends to be in intimate contact with the membrane. Thus, gel expansion occurs in a more extensive volume near the membrane, and growing filaments can still continue to contribute to protrusion without being physically attached to the membrane. Moreover, contributions to protrusive force from filament packing would not be as directly coupled to polymerization or as sensitive to the applied load, especially because energy can be stored transiently by bending while the filament packing is rearranged.

The packing-density mechanism shares some characteristics with the elastic squeezing hypothesis, which proposes that polymerization at the surface of a bacterium such as *Listeria* or an object such

as a vesicle, a bead, or an oil droplet generates stress in the surrounding elastic actin gel, the relaxation of which generates propulsion by squeezing against the object (25). Squeezing results from strains set up in the filament gel as it expands because of polymerization close to the surface and relies on actin cross-linking proteins maintaining the elastic modulus of the gel. Although it has not been possible to determine experimentally the mechanical properties of the MSP filament gel that constitutes the fiber, it is likely that its mechanical strength is lower than that of actin gels, because there do not appear to be analogues of cross-linking protein such as filamin in the nematode motility apparatus. Although the elastic squeezing model clearly contributes to propulsion of curved objects like bacteria and spherical beads (6, 25), it may not make a major contribution to pushing a relatively flat surface such as that represented by the leading edge of a cell. By contrast, gel expansion produced by the decreased filament packing density can also contribute to pushing a relatively flat surface.

In summary, because the maximum packing density of rods decreases with their length, the way elongating filaments pack contributes to the generation of protrusion and complements contributions made by other mechanisms to amoeboid cell motility.

## Materials and Methods

**Preparation of Sperm Extracts for Fiber Assembly.** The S100 cell-free lysate of *Ascaris* sperm was prepared as described (11). Fiber assembly was initiated by addition of ATP (1 mM) to S100 diluted with KPM buffer (0.5 mM $MgCl_{-2}$, 10 mM K phosphate, pH 6.8). Phase-contrast images of fibers were captured on a Zeiss Axioskop2 Plus microscope with a Hamamatsu Orca-ER camera and analyzed with MetaMorph (Molecular Devices) software.

**Electron Tomography.** For electron tomography, fibers were grown in chambers constructed by placing a 22 × 60-mm Thermonox plastic coverslip (Electron Microscopy Sciences) on two parallel strips of three layers of double-sided tape on a 22 × 22-mm glass coverslip. S100 was perfused between the coverslips and fibers allowed to assemble for 10 min, after which they were fixed with 2.5% glutaraldehyde and 0.1% tannic acid in KPM buffer for 30 min. After rinsing with water, samples were postfixed with 1% $OsO_4$ for 30 min, followed by *en bloc* staining with 1% uranyl acetate. Fibers were dehydrated in an ascending ethanol series followed by propylene oxide and embedded in Embed-Araldite resin (Electron Microscopy Sciences). Areas of the plastic wafer containing well preserved fibers were excised and remounted with superglue onto plastic stubs in an orientation suitable for longitudinal sectioning. Semithick (200- to 300-nm) sections were cut on a Ultratome NOVA ultramicrotome, transferred to formvar/carbon-coated copper slot grids, stained with 5% uranyl acetate in 50% methanol followed by Reynold's lead citrate. Tilt series of fibers were acquired over a range of ± 70° at 3° intervals on a Philips CM300 FEG electron microscope equipped with a goniometer, a Gatan Model 670 Ultrahigh tilt analytical holder (Gatan) and a Tem-Cam F224 slow scan CCD camera (Tietz Video). Alignment and refinement of tilt series and back-projection of 3D volumes from tilt series were performed by using a tomography software package developed by Taylor *et al.* (39). The resulting 3D image was imported into AMIRA software for surface rendering, segmentation, and quantitative analyses. To determine the packing density of filaments as a function of distance from the vesicle in tomograms, we defined a grid of 0.1-$\mu$m intervals from the vesicle rearward along the fiber axis and measured the lengths of all filament segments within each interval. Filament length relative to distance from the vesicle was determined by measuring the contour length of all filaments intersected by lines drawn across the fiber normal to and spaced at 0.1-$\mu$m intervals along the fiber axis. These measurements were obtained from tomograms computed from dual-tilt axis datasets of two fibers. We used stereological methods (14) to assess the degree of filament orientation in fibers. Three virtual sections from 3D map data of each of three fiber tomograms were selected by using a random number table. A grid of parallel lines was placed at random on images of these sections and the numbers of filaments (objects with aspect ratio >10) intersecting the lines on the test grid counted. The test grid was rotated and intersect counts repeated at 15° increments from 0° to 180°. Means for the nine intersect counts for each angular increment for each fiber were determined and plotted on polar coordinates. The degree of orientation was calculated as described (14) and analyzed statistically by $\chi^2$ test to evaluate the null hypothesis that the filament orientation is isotropic.

**Engineering and Expression of D83R-MSP.** D83R-MSP was engineered from wild-type $\beta$-MSP cDNA (40) in pET11d (Novagen) by using a Quick Change mutagenesis kit (Stratagene). The mutation was verified by sequencing both strands. The vector was transformed into BL21[DE3] RIL cells. Individual colonies were picked into 2X-TY medium supplemented with 100 $\mu g/ml^{-1}$ ampicillin and grown overnight at 37°C while shaking. Cells were pelleted at 5,000 × *g* for 20 min, lysed with BPER reagent (Pierce), and clarified by centrifugation at 27,000 × *g* for 20 min. The supernatant was dialyzed against 10 mM sodium phosphate, pH 6; 25 mM NaCl; and 0.1 mM PMSF, applied to a Sepharose CM52 cation exchange column, and eluted in a 25–250 mM NaCl gradient. Fractions enriched in D83R-MSP were pooled, concentrated, purified to homogeneity (as judged by SDS/PAGE) over Sephacryl S100 and dialyzed into KPM buffer for polymerization and motility assays.

**Effect of D83R-MSP on Filament Length and Fiber Assembly.** To assess the effect of D83R-MSP on polymerization of purified MSP, we mixed native MSP, obtained as described (24), at 3 $mg/ml^{-1}$ with D83R-MSP at 2 $mg/ml^{-1}$ in KPM containing 30% ethanol (24). As a control, we coassembled native and bacterially expressed wild-type $\beta$-MSP under identical conditions. After 2 min, a 5-$\mu$l aliquot was applied to a carbon-coated EM grid, washed briefly in five drops of 30% ethanol in KPM, negatively stained with 2% aqueous uranyl acetate, and examined with a Philips CM 120 electron microscope. Negatives were digitized and filament contour lengths measured using MetaMorph software. To examine the effect of D83R-MSP on fiber assembly, we perfused fibers growing in S100 diluted 1:5 in KPM buffer with the same material supplemented with 12 $mg/ml^{-1}$ D83R-MSP. The resulting hybrid fibers were examined by light microscopy or prepared for EM tomography as described above. To compare filament packing density in the D83R-MSP and native segments, we measured the lengths of all filament segments contained within 1-$\mu m^2$ boxes (three boxes in each segment of two fibers). Lengths of complete filaments (those for which both ends could be identified unequivocally) in each segment were determined by measuring the end-to-end contour length of filaments that intersected a line down the center of the fiber parallel to the fiber axis. We measured 287 filaments in D83R-MSP segments and 257 filaments in native segments of tomograms of five hybrid fibers.

Hybrid fibers for fluorescence labeling were grown as described above by using S100 supplemented with either native MSP (5 $\mu$M) or D83R-MSP (10 $\mu$M) coupled to Alexa Fluor 488 (Molecular Probes) and purified according to the manufacturer's instructions. Fluorescence images were obtained by using epiillumination and appropriate filter sets for Alexa Fluor 488. Fluorescence intensities in fibers were measured by using MetaMorph software.

We measured the effect of D83R-MSP on fiber growth rate from time-lapse images of fibers obtained before and after the addition of the mutant protein. Rates were calculated by measuring the change in length of fibers from images taken at least 1 min apart. Fiber diameters were determined by measuring the native and D83R-MSP segments of the same hydrid fiber in single phase-contrast images. Changes in fiber contrast were measured as described in ref. 12, and the validity of this method is discussed in detail in *SI Text*. The amount of MSP polymerized, P, was calculated as the volume and density of the cylinder of fiber produced per unit time and was given by:

$$P = (\mathrm{OD}/d) \times d^2 \times v,$$

where OD is the grayscale density at the midpoint of the fiber, *d* is the fiber diameter, and *v* is the velocity.

**ACKNOWLEDGMENTS.** We thank K. A. Taylor for valuable discussions about electron tomography and Lori McFadden for expert technical assistance. This work was supported by National Institutes of Health Grant R37 GM29994. J.L. received postdoctoral support from National Institutes of Health Grant GM64346 to the Cell Migration Consortium. A.W. and A.P. received support from the Stichting voor Fundamentaeel Onderzoek der Materie (FOM), which is part of the Nederlandse Organisatie voor Wetenschappelijk Onderzoek (NOW).

1. Pollard TD, Borisy GG (2003) Cellular motility driven by assembly and disassembly of actin filaments. *Cell* 112:453–465.
2. Small JV, Stradal T, Vignal E, Rottner K (2002) The lamellipodium: where motility begins. *Trends Cell Biol* 12:112–120.
3. Carlier MF, Le Clainche CL, Weisner S, Pantaloni D (2003) Actin-based motility: from molecules to movement. *BioEssays* 25:336–345.
4. Mogilner A, Oster G (2003) Polymer motors: pushing out the front and pulling up the back. *Curr Biol* 13:R721–R733.
5. Condeelis J, Singer RH, Segall JE (2005) The great escape: when cancer cells hijack the genes for chemotaxis and motility. *Annu Rev Cell Dev Biol* 21:695–718.
6. Mogilner A (2006) On the edge: modeling protrusion. *Curr Opin Cell Biol* 17:1–8.

7. Mogilner A, Oster G (2003) Force generation by actin polymerization II: the elastic ratchet and tethered filaments. *Biophys J* 84:1591–1605.
8. Roberts TM, Stewart M (2000) Acting like actin: the dynamics of nematode major sperm protein (MSP) cytoskeleton indicate a push-pull mechanism for amoeboid cell motility. *J Cell Biol* 149:7–12.
9. Theriot J (1996) Worm sperm and advances in cell locomotion. *Cell* 12:1–4.
10. Mogilner A, Oster G (2003) Cell biology: shrinking gels pull cells. *Science* 302:1340–1341.
11. Italiano JE, Roberts TM, Stewart M, Fontana CA (1996) Reconstitution *in vitro* of the motile apparatus from the amoeboid sperm of Ascaris shows that filament assembly and bundling move membranes. *Cell* 84:105–114.
12. Roberts TM, Salmon E, Stewart M (1998) Hydrostatic pressure shows that lamellipodial motility in *Ascaris* sperm requires membrane-associated major sperm protein filament nucleation and elongation. *J Cell Biol* 140:367–375.
13. Medalia O, Weber I, Frangakis AS, Nicastro D, Gerisch G, Baumeister W (2002) Macromolecular architecture in eukaryotic cells visualized by cryoelectron tomography *Science* 298:1209–1213
14. Underwood EE (1970) *Quantitative Stereology* (Addison–Wesley, New York).
15. Philipse AP (1996) (1996) The random contact equation and its implications for (colloidal) rods in packings, suspensions, and anisotropic powders. *Langmuir* 12:1127–1133 [Addendum, *Langmuir* 12:5971.
16. Williams SR, Philipse A (2003) Random packings of spheres and spherocylinders simulated by mechanical contraction. *Phys Rev E* 67:151301.
17. Philipse A, Wierenga AM (1998) On the density and structure formation in gels and clusters of colloidal rods and fibers. *Langmuir* 14:49–54.
18. Roney D, Fivel M, Dendievel R (2005) Discrete modeling of entangled materials. *Phys Rev Lett* 95:108004.
19. Rubinstein M, Colby RH (2003) *Polymer Physics* (Oxford Univ Press, Oxford, UK).
20. Doi M, Edwards SF (1986) *The Theory of Polymer Dynamics* (Oxford Univ Press, Oxford, UK).
21. Doi M (1996) *Introduction to Polymer Physics* (Clarendon Press, Gloucestershire, UK).
22. Bullock TL, McCoy AJ, Kent HM, Roberts TM, Stewart M (1998) Structural basis for amoeboid motility in nematode sperm. *Nat Struct Biol* 5:184–189.
23. Baker AME, Roberts TM, Stewart M (2002) 2.6 Å resolution crystal structure of helices of the motile major sperm protein (MSP) of *Caenorhabditis elegans. J Mol Biol* 319:491–499.
24. King KL, Stewart M, Roberts TM, Seavy M (1992) Structure and macromolecular assembly of two isoforms of the major sperm protein (MSP) from amoeboid sperm of the nematode *Ascaris suum. J Cell Sci* 101:847–857.
25. Plastino J, Sykes C (2005) The actin slingshot. *Curr Opin Cell Biol* 17:62–66
26. Sepsenwol S, Ris H, Roberts TM (1989) A unique cytoskeleton associated with crawling in the amoeboid sperm of the nematode, *Ascaris suum. J Cell Biol* 108:55–66.
27. King KL, Stewart M, Roberts TM (1994) Supramolecular assemblies of the Ascaris suum major sperm protein (MSP) associated with amoeboid cell motility. *J Cell Sci* 107:2941–2949.
28. Xu J, Wirtz D, Pollard TD (1998) Dynamic cross-linking by alpha-actinin determines the mechanical properties of actin filament networks. *J Biol Chem* 273:9570–9576.
29. Tseng Y, An KM, Euse O, Wirtz D (2004) The bimodal role of filamin in controlling the architecture and mechanics of F-actin networks. *J Biol Chem* 279:1819–1826.
30. Svitkina TM, Borisy GG (1999) Arp2/3 complex and actin depolymerizing factor/cofilin in dendritic organization and treadmilling of actin filament array in lamellipodia. *J Cell Biol* 145:1009–1026.
31. Borisy GG, Svitkina TM (2000) Actin machinery: pushing the envelope. *Curr Opin Cell Biol* 12:104–112.
32. Cameron LA, Svitkina TM, Vignjevic D, Theriot JA, Borisy GG (2001) Dendritic organization of actin comet tails. *Curr Biol* 11:130–135.
33. Le Clainche C, Pantaloni D, Carlier MF (2003) ATP hydrolysis on actin-related protein 2/3 complex causes debranching of dendritic actin arrays. *Proc Natl Acad Sci USA* 100:6337–6342.
34. Di Nardo A, Cicchetti G, Falet H, Hartwig JH, Stossel TP, Kwiatkowski DJ (2005) Arp2/3 complex-deficient mouse fibroblasts are viable and have normal leading-edge actin structure and function. *Proc Natl Acad Sci USA* 102:16263–16268.
35. Orlova A, Egelman EH (1993) A conformational change in the actin subunit can change the flexibility of the actin filament. *J Mol Biol* 232:334–341.
36. De La Cruz EM, Mandinova A, Steinmetz MO, Stoffler D, Aebi U, Pollard TD (2000) Polymerization and structure of nucleotide-free actin filaments. *J Mol Biol* 295:517–526.
37. Dickinson RB, Caro L, Purich DL (2004) Force generation by cytoskeletal filament end-tracking proteins. *Biophys J* 87:2838–2854.
38. Alberts JB, Odell GM (2004) *In silico* reconstitution of Listeria propulsion exhibits nano-saltation. *PLoS Biol* 2:e412.
39. Taylor KA, Tang J, Cheng Y, Winkler H (1997) The use of electron tomography for structural analysis of disordered protein arrays. *J Struct Biol* 120:372–386.
40. Bullock TL, Parthasarathy G, Kent H, Roberts TM, Stewart M (1996) New crystal forms of the motile major sperm protein (MSP) of *Ascaris suum. J Struct Biol* 116:432–437.